Nanoscale

ROYAL SOCIETY OF CHEMISTRY

PAPER

View Article Online
View Journal | View Issue

Cite this: *Nanoscale*, 2020, **12**, 14204

Tunable electrochromic behavior of titanium-based MXenes†

Geetha Valurouthu, Kathleen Maleski, Narendra Kurra, Meikang Han, Kanit Hantanasirisakul, Asia Sarycheva and Yury Gogotsi *

Two-dimensional transition metal carbides, nitrides and carbonitrides, popular by the name MXenes, are a promising class of materials as they exhibit intriguing optical, optoelectronic and electrochemical properties. Taking advantage of their metallic conductivity and hydrophilicity, titanium carbide MXenes ($Ti_3C_2T_x$ and others) are used to fabricate solution processable transparent conducting electrodes (TCEs) for the design of three-electrode electrochromic cells. However, the tunable electrochromic behavior of various titanium-based MXene compositions across the entire visible spectrum has not yet been demonstrated. Here, we investigate the intrinsic electrochromic properties of titanium-based MXenes, $Ti_3C_2T_x$, Ti_3CNT_x, Ti_2CT_x, and $Ti_{1.6}Nb_{0.4}CT_x$, where individual MXenes serve as a transparent conducting, electrochromic, and plasmonic material layer. Plasmonic extinction bands for $Ti_3C_2T_x$, Ti_2CT_x and $Ti_{1.6}Nb_{0.4}CT_x$ are centered at 800, 550 and 480 nm, which are electrochemically tunable to 630, 470 and 410 nm, respectively, whereas Ti_3CNT_x shows a reversible change in transmittance in the wide visible range. Additionally, the switching rates of MXene electrodes with no additional transparent conductor electrodes are estimated and correlated with the respective electrical figure of merit values. This study demonstrates that MXene-based electrochromic cells are tunable in the entire visible spectrum and suggests the potential of the MXene family of materials in optoelectronic, plasmonic, and photonic applications, such as tunable visible optical filters and modulators, to name a few.

Received 4th April 2020,
Accepted 10th June 2020

DOI: 10.1039/d0nr02673e

rsc.li/nanoscale

Introduction

Recent technological trends towards development of smart windows, flat panel displays, and wearable textiles have advanced the field of electrochromic energy storage.[1,2] Electrochromism is a phenomenon that involves the dynamic change of colors or optical properties of materials in response to applied electric charge.[3,4] However, poor electronic conductivity and degradation associated with reversible ion intercalation have been the major issues with conventional electrochromic materials.[5] Therefore, efforts are being made, focusing on developing new types of electrochromic devices that can exploit the plasmonic properties of materials.[5–8] Specifically, plasmonic materials with reversible redox capability offer electrochemically tunable optical properties. Plasmonic electrochromic devices in the near infrared (NIR) range have been demonstrated by employing transparent conducting oxide nanocrystals or combining with plasmonic metal nanoparticles.[3,9] Tunable electrochromic behavior in the visible spectrum of wavelengths is appealing due to its implications in developing flat panel displays and smart windows.[10] Conventional electrochromic materials, W_xO_y combined with polyoxometalates have been demonstrated for visible electrochromic devices.[11] However, it is challenging to develop active electrodes that combine various properties such as optoelectronic, plasmonic, and redox type characteristics in a single material. Moreover, there is a stringent requirement focused on having the redox processes occur within the electrochemical stable potential window, while simultaneously tuning the plasmonic behavior reversibly without electrochemical corrosion effects.

Transition metal carbides, nitrides and carbonitrides (MXenes) are a rapidly growing class of conductive two-dimensional (2D) materials, suitable for a wide range of applications including electrochemical energy storage, gas sensors and electronics.[12,13] For instance, the representative member of the MXene family, $Ti_3C_2T_x$, with excellent optoelectronic properties and metal-like free electron density, opened doors for new types of applications such as plasmonics, photonic diodes, electromagnetic interference shielding and spray-on antennas.[14–18] The available 2D MXene galleries with wide interlayer spacing and redox active sites of the transition metal

A. J. Drexel Nanomaterials Institute and Department of Materials Science and Engineering, Drexel University, Philadelphia, PA 19104, USA.
E-mail: gogotsi@drexel.edu

†Electronic supplementary information (ESI) available. See DOI: 10.1039/d0nr02673e

oxide-like surface are key for high rate pseudocapacitive energy storage.[19,20] Surface plasmon extinction properties, combined with optical transparency, conductivity and redox properties, make MXene materials an attractive platform for plasmonic electrochromic devices.[21,22] Salles *et al.* demonstrated the electrochromic effect in $Ti_3C_2T_x$ MXenes through reversible change of the redox state of titanium by (de) protonation of oxygen containing functional groups (=O and –OH).[15] El-Demellawi *et al.* investigated the change of surface plasmon energies of $Ti_3C_2T_x$ by controlling surface terminations through thermal desorption of fluorine functional groups.[22] In recent systematic studies on optical properties with respect to MXene compositions, a wide range of optical signatures are noticed.[23–25] This motivated us to investigate different titanium-based MXenes for electrochromic applications and to probe how transition metal composition can be used to tailor light absorption to specific wavelengths of interest, especially in the visible range.

In this study, we used four different titanium-based MXene thin films to study the dependence of the transition metal composition, stoichiometry, and optoelectronic characteristics on the resulting electrochromic performance. Among the dozens of available MXenes, as a proof concept, we have chosen $Ti_3C_2T_x$, Ti_3CNT_x, Ti_2CT_x and $Ti_{1.6}Nb_{0.4}CT_x$ for studying the electrochromic effect. Due to the difference in the optical properties of MXenes, we were able to demonstrate tunable electrochromic behavior over the entire visible spectrum. The electrochromic effect is primarily governed by the surface redox reactions of the titanium (transition metal) surface, while the switching rates of the proposed three-electrode cells are mostly dependent on the optoelectronic quality (electrical figure of merit) of the MXene thin films.

Results and discussion

The unique combination of metallic conductivity and hydrophilicity makes MXenes a versatile class of materials for emerging optical and optoelectronic applications.[14,25] Spray-coated MXene thin films appear to be visually distinct as shown in Fig. 1a (pale greenish – $Ti_3C_2T_x$, dim grayish – Ti_3CNT_x, pale magenta – Ti_2CT_x, and tan brown – $Ti_{1.6}Nb_{0.4}CT_x$). The inherent surface functionality (=O, –F, –OH, and –Cl) results from the etching and delamination of the MAX precursor, which imparts negative surface charges (zeta potential of less than −30 mV at a neutral pH of 6–7), enabling stable dispersions in water without additional surfactants (Fig. S1a and b, ESI†). Such stable colloidal dispersion of MXenes can be solution-processed to make conductive films or coatings *via* vacuum-assisted filtration, spray, spin and dip-coating methods.[26] As shown in Fig. 1a, four different titanium-based MXene compositions ($Ti_3C_2T_x$, Ti_3CNT_x, Ti_2CT_x and $Ti_{1.6}Nb_{0.4}CT_x$) were processed in the form of transparent thin films by a spray coating method. Typical lateral dimensions of MXene flakes were estimated using DLS, which are found to be ~1 μm (Fig. S1c and d, ESI†).

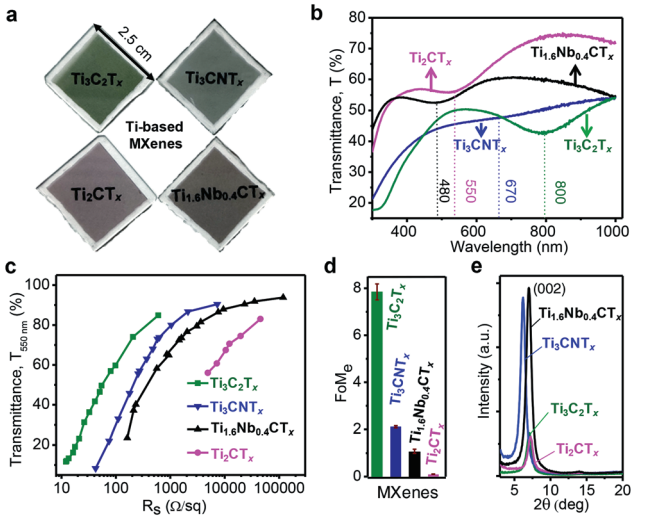

Fig. 1 Optical and optoelectronic properties of titanium-based MXene thin films ($Ti_3C_2T_x$, Ti_3CNT_x, Ti_2CT_x, and $Ti_{1.6}Nb_{0.4}CT_x$). (a) Digital photographs showing a visual contrast among transparent MXene thin films processed by spray coating and (b) corresponding UV-vis spectra showing extinction characteristics over the entire visible range, relevant extinction band positions are marked. (c) Relationship between transmittance at 550 nm ($T_{550\ nm}$) *versus* sheet resistance (R_s). (d) Estimated electrical figure of merit (FoM_e) values for MXene thin films, and (e) their XRD patterns showing (002) reflection.

To study the optical properties of MXene thin films, UV-vis-NIR spectra were recorded in the range of 300–1000 nm (Fig. 1b). MXene thin films have broad extinction peaks at different wavelengths in the visible range, specific to the MXene composition. The extinction characteristics are governed by the composition and stoichiometry of transition metals, carbon and/or nitrogen. However, based on synthesis and processing conditions, the given MXene composition may have slight variations in the optical properties. The extinction peaks for $Ti_3C_2T_x$, Ti_2CT_x and $Ti_{1.6}Nb_{0.4}CT_x$ are observed at ~800 nm, ~550 and 480 nm, respectively, while an inflection is observed for Ti_3CNT_x at 670 nm. Therefore, the composition-dependent extinction characteristics of titanium-based MXenes can be utilized to cover the entire visible spectrum. The optical extinction peak at ~800 nm for $Ti_3C_2T_x$ has been attributed to the surface plasmon resonance, in particular – transverse plasmon resonance in the visible region of the electromagnetic spectrum.[22,27] Assuming that the same mechanism holds true for the optical extinction peak in other MXenes, the position of the transverse plasmon resonance is highly dependent on the MXene composition as their peak positions are observed at the different wavelengths when the composition changes.

The optoelectronic properties of MXene thin films were estimated by an electrical figure of merit (FoM_e), a dimensionless quantity correlating optical transparency and sheet resistance (R_s) values. FoM_e is often used to quantify the optoelectronic quality of transparent conducting electrodes (TCEs) and is defined by the ratio of DC electrical conductivity (σ_{DC}) to optical conductivity (σ_{op}) of the TCEs.[21] Here, the FoM_e is an

average of the values obtained from eqn (1) by measuring the transmittance at 550 nm ($T_{550\ nm}$) and the sheet resistance (R_s) of MXene thin films of different thicknesses (5–120 nm) for each composition.

$$T_{550\,nm} = \left(1 + \frac{188.5}{R_s}\frac{\sigma_{op}}{\sigma_{DC}}\right)^{-2} \quad (1)$$

FoM_e for the MXene thin films is highly dependent on several parameters, such as the MXene composition, and synthesis and processing conditions. Since a spray-coating technique was used to fabricate all MXene thin films, the effect of film processing on the difference of FoM_e was ruled out. Therefore, FoM_e is mostly governed by the intrinsic electrical conductivity and optical properties.[27] MXene thin films followed a common trend of percolative electrical transport (decrease in sheet resistance with the decrease in transparency) in a low sheet resistance value regime and then bulk-like electrical transport (sheet resistance is nearly constant with the decrease in transparency) as shown in Fig. 1c.[15] $Ti_3C_2T_x$ has a much higher FoM_e value of 7.8 compared to Ti_3CNT_x (FoM_e = 2.1) Ti_2CT_x (FoM_e = 0.1) and $Ti_{1.6}Nb_{0.4}CT_x$ (FoM_e = 1). As shown in Fig. 1d, FoM_e values for $M_3X_2T_x$ compositions are higher compared to M_2XT_x, which could be attributed to the lower oxidation state and free electrons in the inner layer of Ti atoms in $M_3X_2T_x$.[28] It is important to note that this FoM_e was calculated at 550 nm and could change with the wavelength of interest. This wavelength was chosen to compare the studied MXenes and materials reported in the literature. $Ti_3C_2T_x$ thin films showed superior optoelectronic quality over the rest of the titanium-based MXenes, in part due to well-developed synthesis conditions and optimal surface chemistry of $Ti_3C_2T_x$. However, all titanium-based MXene thin films (thickness, 40 nm) showed good crystalline quality as evident from the strong (002) reflection peak, as shown in Fig. 1e. The (002) reflection around 6.5–7.2° in MXenes corresponds to a *d*-spacing of 13.4–12.2 Å which is sufficiently large for protons to access the surface terminations with subsequent redox reactions with rapid kinetics.

Optoelectrochemical characteristics of MXene thin films were investigated using a three-electrode electrochemical cell combined with UV-vis-NIR measurements. As shown in Fig. 2a, Ag wire and a 100-nm-thick $Ti_3C_2T_x$ film (Fig. S2, ESI†) were employed as a quasi-reference electrode (RE) and a counter electrode (CE), respectively.[15] In order to probe the optical properties of the working electrode (WE), a circular area of ~7 mm diameter was scratched off from the counter electrode where incident light can pass through the CE and WE without significant optical extinction from the CE, as shown in Fig. 2b.

Cyclic voltammograms (CVs) of MXene thin films with different compositions are displayed in Fig. 2c. It is observed that the semi-transparent MXene thin films deviate from the rectangular CV profiles, probably due to resistive behavior over free-standing thick films. However, the magnitude of redox behavior of a MXene thin film is governed by the extent of charge transfer with the electrolyte ions. $Ti_3C_2T_x$, Ti_3CNT_x, Ti_2CT_x, and $Ti_{1.6}Nb_{0.4}CT_x$ thin films showed different CV profiles, providing a clue that all MXenes have their own unique signatures of redox behavior. Optical properties are dictated by the redox nature, that is, different MXenes have different optical extinction properties. The Faradaic current from oxidation/reduction reactions primarily governs the color change or switching in redox-based electrochromic cells.[29] Areal charge capacitances

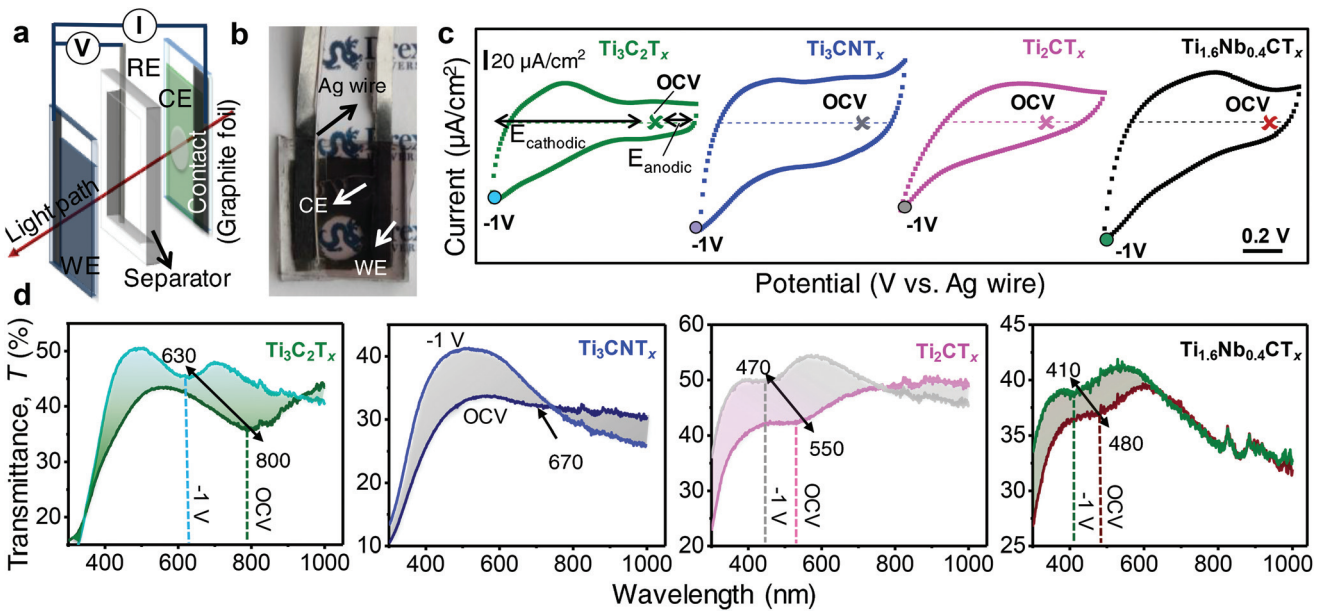

Fig. 2 *In situ* opto-electrochemical characterization of MXene thin film three-electrode cells. (a) Schematic illustration of three-electrode device set-up and (b) its corresponding digital photograph. (c) Typical cyclic voltammograms (CVs) of MXene thin films ($Ti_3C_2T_x$, Ti_3CNT_x, Ti_2CT_x and $Ti_{1.6}Nb_{0.4}CT_x$) at 20 mV s^{-1} and (d) their optical extinction properties at cathodic polarization (–1 V *vs.* Ag wire) with respect to open circuit voltage (OCV).

of MXene thin films were estimated by integrating the discharge portion of the CVs (eqn (E1), ESI†), and the typical values at a scan rate of 20 mV s^{-1} were found to be 3.92, 1.87, 1.36 and 2.21 mF cm^{-2} for $Ti_3C_2T_x$, Ti_3CNT_x, Ti_2CT_x and $Ti_{1.6}Nb_{0.4}CT_x$ thin film devices, respectively.

The electrochromic behavior of MXene thin films was studied by recording *in situ* UV-vis-NIR spectra by imposing constant potentials (chronoamperometry) simultaneously. To take advantage of the proton-induced pseudocapacitive behavior of MXenes, a protic gel electrolyte was used. For each cell, UV-vis-NIR spectra were recorded starting from open circuit voltage (OCV) to −1 V (cathodic polarization) followed by anodic sweep up to 0.1 V (*vs.* Ag wire) in steps of 100 mV. Cathodic ($E_{cathodic}$) and anodic (E_{anodic}) polarizations are defined with respect to OCV as marked in Fig. 2c. The changes in optical properties driven by the cathodic polarization of MXene thin film electrodes are displayed in Fig. 2d where a blue shift in the extinction spectra of MXene electrochromic devices was observed. During the cathodic polarization, the $Ti_3C_2T_x$ extinction peak shifts from 800 nm (at OCV) to 630 nm (at −1 V *vs.* Ag wire) with 8.6% increase of transmittance at 800 nm. Upon gradual increase of cathodic potential from OCV, it was observed that the extinction peak slowly shifts towards lower values of wavelengths (higher energy) (Fig. S3a, ESI†). It is known that the titanium surface is reduced by protonation of oxygen functionalities with subsequent reduction of the Ti oxidation state, as confirmed by previous studies.[30] In order to probe the mechanism of electrochromic behavior, XPS may be helpful, but it is limited by the *ex situ* nature of those measurements. Protonated oxygen surface termination is only maintained under imposed cathodic potentials to the MXene electrodes. Since we observed a spontaneous extinction peak shift to its original value (at OCV) as soon as the potential was removed from the electrodes (Fig. S3, ESI†), *ex situ* XPS measurements were futile. With the reversal of polarization from −1 V (*vs.* Ag wire) to OCV, the extinction peak red-shifted back towards its original position, confirming the highly reversible nature of the Ti-redox state. At anodic potentials within the stable regime, no shift of the extinction peak was observed (Fig. S3c, ESI†). This is due to electrostatic (de)sorption of ions (from) onto $Ti_3C_2T_x$ without a change of the Ti oxidation state.

A visual color change from pale green (at OCV) to blue (at −1 V *vs.* Ag wire) is clear from the digital video taken during cathodic sweeps (Fig. S4 and Video V1, ESI†). The reversible electrochromic behavior of $Ti_3C_2T_x$ was also further confirmed by relaxing the system to the equilibrium state after imposing the potentials (insets of Fig. S3a and c, ESI†). The improved electrochromic behavior in our case can be attributed to the variations in the synthesis, processing and cell-design engineering parameters. For instance, Salles *et al.* reported an optical shift from 670 to 770 nm (optical shift of 100 nm) for $Ti_3C_2T_x$ films processed by a dip-coating method, when the MILD (HCl and LiF) method was employed to prepare $Ti_3C_2T_x$.[15] Probably, differences in the synthesis protocol resulted in different amounts of surface functional groups, such as an increase in active redox sites (increased amount of oxy functional groups compared to fluorine), or changes in the carrier concentration of the thin film investigated, which influenced the plasmonic peak position. Various classes of materials showed tunable maximum plasmonic shifts in the range of 17–192 nm; Ag NPs (17 nm),[31] PANI-Au/ITO (70 nm),[32] PEDOT-Au/ITO (192 nm),[33] WO_3/Ag NPs (30 nm),[34] polythiophenes/Au NPs (12 nm),[35] Au nanocubes/PANI (25 nm)[36] and Au nanobipyramids/PANI (150 nm).[37] Plasmonic nanoparticles typically exhibit a double layer charging mechanism; however, coupling with redox active conductive polymers and metal oxides enhanced the plasmonic spectral shifts as is evident from the above examples.[38] In this scenario, MXenes stand as a unique class of materials which simultaneously exhibit plasmonic and conducting redox charging properties, and hence circumvent the use of a transparent current collector, like ITO.

To study the effect of the transition metal composition and stoichiometry on electrochromic behavior, three different titanium-based MXenes were compared. A reversible onset of extinction (inflection point) at 670 nm (OCV) gradually disappears during cathodic sweep (−1 V *vs.* Ag wire) for Ti_3CNT_x (Fig. 2d). The broad reversible transmittance changes of 6.3–10% at 600–400 nm are observed during cathodic sweep (OCV to −1 V *vs.* Ag wire). The gradual damping of the onset at 670 nm of Ti_3CNT_x driven by small increments in applied cathodic potentials is shown in Fig. S3d, ESI.† The dim grayish MXene thin film became slightly transparent with violet tint (Fig. S4, ESI†), as shown in Video V2, ESI† captured under cathodic polarization.

In the case of Ti_2CT_x thin films, a shift from 550 nm (OCV) to 470 nm (−1 V *vs.* Ag wire) is observed, supporting the change of the Ti oxidation state (Fig. 2d). Interestingly, the UV transmittance increased by 10% during the cathodic polarization of Ti_2CT_x thin films at 550 nm. Similarly, for $Ti_{1.6}Nb_{0.4}CT_x$ thin films, a shift from 480 nm (OCV) to 420 nm (−1 V *vs.* Ag wire) is observed and 8.5% change in transmittance (optical contrast) at 480 nm is displayed (Fig. 2d). The visual change in optical properties is more significant in $Ti_{1.6}Nb_{0.4}CT_x$ than Ti_2CT_x thin films, going from wine brownish or magenta at OCV to a transparent film with a green tint at −1 V *vs.* Ag wire during cycling, as shown in Fig. S4, Videos V3 and V4, ESI.† It is clear that there is a change in optical properties of MXene thin films based on the spectral shift, but the color switching is not clearly distinguishable by the naked eye. This could be attributed to the high electrical resistance of the Ti_2CT_x thin films or the wavelength, which is approaching the limit of what the human eye can distinguish (~400 nm). Similar to the $M_3X_2T_x$ phase, there is no significant shift observed during anodic polarization when cycled within the electrochemical stability window. To confirm that the reversible color change is due to the change of the redox state of Ti, we anodically oxidized a $Ti_3C_2T_x$ thin film by sweeping to 0.8 V (*vs.* Ag wire) (Fig. S5, ESI†). At this stage, Ti was irreversibly oxidized to +4 state (TiO_2) with loss of spectroelectrochemical activity on further cathodic polarization.[39] It is evident from

the observations that the MXenes studied are cathodic coloring materials and exhibit plasmonic electrochromic effects. The blue shift in the extinction properties of titanium-based MXenes can be attributed to an increased electronic density of titanium atoms (in the reduced state) under cathodic polarization. It is hypothesized that the reduction of the titanium surface at cathodic potentials increases the electron density on titanium atoms and causes the blue shift in the extinction peak.

Since we are using acidic electrolytes, protons, being the smallest cations, can get intercalated even into the compacted MXene films causing redox reactions. However, wider interlayer spacing offers faster access to the electrochemically active surface area. It was shown that the origin of the optical peak shift is not because of change of interlayer spacing due to intercalation/de-intercalation of H^+ ions.[22] Therefore, even the compact MXene thin films can show electrochromic behavior as long as redox reactions are possible.

In addition to the shift in the optical extinction band, we have also observed transmittance changes in the MXene thin films under applied cathodic potentials. The specific wavelengths were chosen (for each type of MXene) where a maximum change of transmittance was observed. As evident from Fig. 2c, $Ti_3C_2T_x$, Ti_3CNT_x, Ti_2CT_x and $Ti_{1.6}Nb_{0.4}CT_x$ thin film electrodes showed maximum change in the transmittance values at 500, 480, 380 and 350 nm, respectively. In the case of $Ti_3C_2T_x$, a reversible transmittance change of up to 8% was observed for more than 2000 cycles as shown in Fig. 3a. Similarly, for Ti_3CNT_x, reversible transmittance changes up to 6.8% was observed which subsequently dropped to 4.3% after ~1000 cycles. The change of transmittance is attributed to change in the electronic state of the MXene. This change is reversible upon electrochemical redox cycle. Therefore, protonation of the MXene surface causes a change in the electronic structure, and hence the optical properties of the MXene films. *In situ* Raman and electron energy loss spectroscopy studies have investigated plasmonic behavior of Ti_3C_2.[15,22] We assume that a similar mechanism is valid for other MXene compositions too.

However, in the case of Ti_2CT_x, and $Ti_{1.6}Nb_{0.4}CT_x$ thin film electrodes, irreversible transmittance variations were observed with the cycle number. There was a decrease in the ΔT in the initial cycles followed by the increase of the transparency level of their respective working electrode films. This could be due to electrochemical oxidation induced degradation or prolonged contact of M_2XT_x MXene thin films with aqueous-based electrolytes.[40] Moreover, thin films (tens of nm) are more prone to oxidation compared to thick films (hundreds of nm). Hysteresis in charge and discharge capacitances with the cycle number is also an indication of irreversible chemical changes resulting in irreversible transmittance change, which is shown in the case of Ti_2CT_x (Fig. S6, ESI†).

Switching time of the electrochromic three-electrode cell is estimated by measuring the time required to change the transmittance by 90% of ΔT (Fig. S7, ESI†). For the sake of better ionic conductivity and transport, a liquid electrolyte (1 M H_3PO_4) was chosen over the gel electrolyte. As shown in Fig. 3b, the switching times of titanium-based electrochromic systems are plotted with the wavelength shift, indicating tunable electrochromic behavior in the visible spectrum. Switching times of $Ti_3C_2T_x$, Ti_3CNT_x, Ti_2CT_x, and $Ti_{1.6}Nb_{0.4}CT_x$ thin film electrodes are estimated to be ~0.7, 1.2, 14, and 1.5 s, respectively. The fast response of the $Ti_3C_2T_x$ electrochromic cell and rapid extinction change per volt (230 nm V^{-1}) are governed by its low sheet resistance value with a higher FoM_e compared to the other MXenes studied. We have estimated the extinction spectral shift (electro-optical capacitance) from the slope obtained from a region where there is a linear increase of plasmon resonance energy with respect to potential (Fig. 3c). The estimated electro-optical capacitances are found to be 230 nm V^{-1}, 100 nm V^{-1} and 165 nm V^{-1} for $Ti_3C_2T_x$, Ti_2CT_x and $Ti_{1.6}Nb_{0.4}CT_x$, respectively. These values are higher than those of metal-nanoparticle based electrochromic devices, due to the pseudocapacitive behavior of MXenes. As evident from Fig. 3b, the optical properties (transmittance and spectral shift) of titanium-based MXenes are electrochemically tunable in the visible range of the electromagnetic spectrum (800 to 400 nm). The extent of shift is based on accessible Ti active redox sites capable of changing their electron density upon electrochemical charging.

Fig. 3c estimates the change of the peak position (converted to energy, eV) of MXene electrochromic systems with respect to different compositions and cathodic potentials. While it is clear that each respective MXene composition operates in a different wavelength window, the corresponding optical shifts in energy are similar (0.42 eV for $Ti_3C_2T_x$, 0.37 eV for Ti_2CT_x,

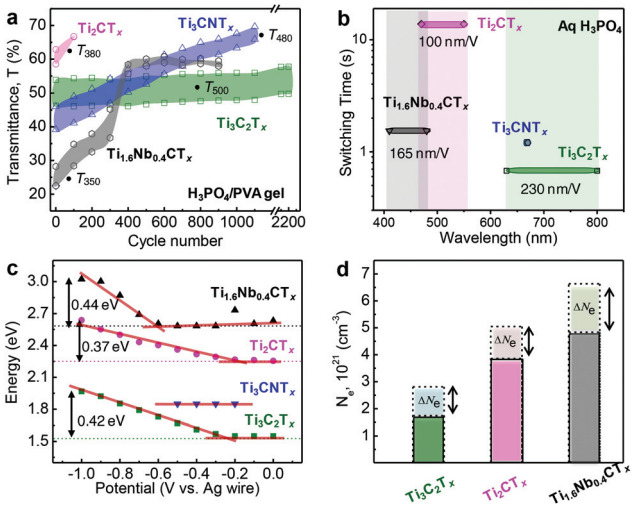

Fig. 3 Electro-optical responses of titanium-based MXene electrodes. (a) Change of transmittance recorded at a specific wavelength of 500, 480, 380 and 350 nm, respectively for $Ti_3C_2T_x$, Ti_3CNT_x, Ti_2CT_x, and $Ti_{1.6}Nb_{0.4}CT_x$ MXene electrochromic cells with the cycle number. (b) Switching time *versus* wavelength, (c) variation in plasmon resonance energy of MXene thin films at cathodic potentials with respect to the OCV state (shown in dotted line) and (d) the estimated relative variations in electron densities of titanium-based MXenes, under applied cathodic potentials, *i.e.*, compared between OCV and −1 V *vs.* Ag wire.

and 0.44 eV for $Ti_{1.6}Nb_{0.4}CT_x$). Correlating this to an estimation of the free electron density, or carrier concentration (N_e), blue shifts with the injection of electrons through electrochemical cycling can be plotted (Fig. 3d) *via* the relationship that the peak position is proportional to $\sqrt{N_e}$ (eqn (E2), ESI†).[41,42] When comparing the predicted carrier concentration values at OCV and under cathodic potential (−1 V *vs.* Ag wire), an increase in carrier concentration can be estimated. The magnitude of the change, however, is inversely proportional to the magnitude of shift in nanometers, an important consideration when deciding on a MXene to use in a specific wavelength region. While $Ti_3C_2T_x$ exhibits the largest shift in wavelength, the corresponding change in the electron density is the lowest, while the opposite is shown for $Ti_{1.6}Nb_{0.4}CT_x$. It is important to focus on future studies in evaluating and monitoring the experimental changes in carrier concentration of these MXene films to understand the fundamental relationships between the free electron densities and MXene composition. This would allow one to further tune electrochromic three-electrode cell performance. Please note that relative carrier concentrations and plasmon energy changes were estimated purely based on optical measurements with some approximations. This analysis allows us to compare our materials investigated in this study but may not be directly applicable to comparison with other systems. Taking into account that at least 30 stoichiometric MXene compositions and numerous solid solutions have been reported, it is possible to develop MXene-based optical filters with tunable optical properties over the entire visible and IR spectrum. Moreover, due to the high conductivity of MXenes, the use of transparent conductors like ITO is not required, enables manufacturing of devices on a variety of substrates, including flexible ones.

This study demonstrates the proof of concept of color change in MXene thin films without employing external TCEs. This study greatly expands the electrochromic spectral window for MXene thin films and opens opportunities for transition metal carbides and/or nitrides in optoelectronic applications.

Conclusions

Electrochromic effects of titanium-based MXene thin films were studied by employing $Ti_3C_2T_x$, Ti_3CNT_x, Ti_2CT_x, and $Ti_{1.6}Nb_{0.4}CT_x$ thin films of optoelectronic quality. The optical extinction properties of titanium-based MXene thin films were reversibly tuned under cathodic potentials, where surface redox reactions are prominent and dominate over conventional double layer charging. The maximum electro-optical shifts were 170, 80 and 70 nm for $Ti_3C_2T_x$, Ti_2CT_x and $Ti_{1.6}Nb_{0.4}CT_x$, respectively. The switching rates of the MXene electrochromic cells were in the range of 0.7 to 14 s, which were governed by their corresponding electrical figure of merit as there was no external TCE employed. Thus, titanium-based MXenes are capable of exhibiting tunable plasmonic properties in the visible range of wavelengths.

Experimental

Synthesis of MXene colloidal suspensions

The detailed procedure for MAX phase synthesis is provided in the ESI.†

$Ti_3C_2T_x$ MXene. A minimal amount of hydrofluoric acid (HF, Fisher, technical grade, 48–51 wt%), *ca.* 5 wt%, was used for etching the Ti_3AlC_2 MAX phase as reported previously.[18] The etching solution contains 12 mL concentrated hydrochloric acid (HCl, Fisher, technical grade, 35–38%), 6 mL deionized (DI) water and 2 mL of concentrated HF. While stirring at 340 rpm, 1 g of Ti_3AlC_2 powder was slowly added into a vial and stirred continuously for 24 h at room temperature. After the etching reaction, washing was conducted with DI water several times *via* centrifugation for 5 min each at 3500 rpm, followed by decantation of the clear, acidic supernatant. This step was repeated until neutral pH of 6–7 was achieved.

The wet slurry containing multilayer $Ti_3C_2T_x$ was added into a solution of 1 g lithium chloride (LiCl, Alfa Aesar, 98+%) in 50 mL of DI water followed by manual shaking for 5 min and constant stirring (200 rpm) for 4 h at room temperature.[18] During this intercalation process, hydrated Li-ions intercalate between multilayer lamellas, weakening the out-of-plane nanosheet interactions delaminating into individual MXene flakes. The suspension was washed with DI water (300 mL) by centrifuging and decanting the supernatant until a dark supernatant was obtained. Swelling behavior of MXenes (clay-like behavior) was observed due to intercalation of Li-ions and water molecules. After redispersion of the swollen sediment, a stable dark supernatant of $Ti_3C_2T_x$ was collected after 30 min of centrifugation at 3500 rpm. The concentration of the $Ti_3C_2T_x$ colloidal suspension was measured by filtering the solution through a polypropylene filter (3501 Coated PP, Celgard LLC, Charlotte, NC), followed by drying under vacuum at 70 °C overnight.

Ti_2CT_x MXene. A Ti_2CT_x MXene colloid was prepared similarly to the $Ti_3C_2T_x$ MXene colloid with slight modifications in the etching and delamination protocol. Addition of the Ti_2AlC MAX phase to the etching media is highly exothermic so to prevent overheating during the addition, the vial is placed in an ice bath. The Ti_2AlC MAX phase was added carefully in small quantities to the etching solution placed in an ice bath. Stirring time for etching was reduced to 20 h at room temperature as it is easier to etch the Ti_2AlC MAX phase compared to Ti_3AlC_2. Delaminating Ti_2CT_x MXene is also usually faster, so after the addition of 1 g of LiCl, 30 min of handshaking was enough to obtain the delaminated Ti_2CT_x MXene. The washing and collection of dark colloidal Ti_2CT_x dispersion steps remained the same as those for $Ti_3C_2T_x$.

Ti_3CNT_x and $Ti_{1.6}Nb_{0.4}CT_x$ MXenes. Ti_3CNT_x and $Ti_{1.6}Nb_{0.4}CT_x$ MXene colloids were individually prepared by selective etching of Al from Ti_3AlCN and $Ti_{1.6}Nb_{0.4}AlC$ MAX phases following the minimally intensive layer delamination (MILD) approach reported by Alhabeb *et al.* with slight modifications in the etching duration as reported elsewhere.[26,43] In short, 1 g of MAX phase was added to the etching media comprising

lithium fluoride salt (1.5 g) (LiF, Alfa Aesar, >98%) dissolved in hydrochloric acid (10 mL) (HCl, Fisher, technical grade, 35–38%) and DI water (10 mL) under continuous stirring for 24 h and 48 at 35 °C to obtain Ti_3CNT_x and $Ti_{1.6}Nb_{0.4}CT_x$ MXenes, respectively. The resulting acidic media were washed with DI water by successive centrifugation for 5 min at 3500 rpm and decanting the supernatant until the supernatant became dark followed by centrifugation for 5 min at 9000 rpm and decanted supernatant until pH 6 is reached. Meanwhile, expansion in the MXene sediment was observed as an indication of delamination. After 6–7 washing steps (total of 500 mL), the resulting neutral media were centrifuged for 10 min at 3500 rpm and the dark supernatant of the MXene colloid was collected and used for spray coating.

Spray-coating of MXene thin films

Microscopic glass slides of 25 × 75 × 1 mm (Fisher Scientific) were cleaned by sequential bath sonication (Branson 2510 Ultrasonic Cleaner, 100 W) in detergent solution (Hellmanex III, Fisher Scientific) to remove any residue followed by DI water and ethanol successively for 15 minutes each and then dried by blowing compressed air. The cleaned glass substrates were then plasma treated (Tergeo Plus, Pie Scientific) at 150 W with O_2 flow at 4 sccm for 5 minutes to make the glass surface hydrophilic. A spray coating technique was adopted to process MXene colloids into thin films, due to the ease in controlling thickness by varying concentration of the colloid and number of coatings. The pre-treated glass substrates were spray-coated with MXene colloids followed by air drying after every layer of coating by blowing through a hair dryer (Conair brand – 1875). The amount of colloids used in spray-coating was varied to produce films with thicknesses ranging from 15–160 nm, keeping the MXene dispersion concentration at 2 mg mL^{-1}. MXene thin films were kept in a vacuum desiccator overnight before performing characterization.

Electrolytes

The electrolytes used were 1 M phosphoric acid in polyvinyl alcohol gel (H_3PO_4/PVA gel) and 1 M phosphoric acid (H_3PO_4). 1 g of polyvinyl alcohol (PVA, Alfa Aesar, 98%) was dissolved in 10 mL of DI water at 85 °C under stirring for 3 h at 340 rpm after which a transparent gel was obtained.[44] 1 g (0.6 mL) of concentrated H_3PO_4 (Alfa Aesar) was added to 10 wt% PVA gel and stirred for 30 min to obtain 1 M H_3PO_4/PVA gel electrolyte.

Encapsulation of electrochemical cells

For opto-electrochemical characterization, a three-electrode configuration was employed. Semi-transparent MXene thin films with different compositions (~30–50% transparency at 550 nm, thickness ~40–50 nm) were used as working electrodes (WE), silver wire as a pseudo-reference electrode (RE) and a $Ti_3C_2T_x$ thick film (~100 nm) as a counter electrode (CE). An electrochromic cell (2.5 cm × 2.5 cm) is designed in such a way that it fits in the sample-holder of the UV-Vis spectrophotometer to carry out *in situ* measurements. In order to avoid optical contribution from the counter electrode, the thick $Ti_3C_2T_x$ electrode film was gently scratched in the center (creating a hole/gap in the thin film) to allow the UV-vis incident beam to only pass through the working electrode.[44] 3M Double sided tape (3M™ VHB™ Tape 4910) was used as a spacer to hold the electrolyte and attach to the electrodes to provide mechanical robustness to the electrochromic three-electrode set-up. We used 2 mm wide graphite foil-strips (0.13 mm thick, Alfa Aesar) to extend the MXene contacts for electrical connection with the electrochemical workstation. MXene thin films of similar transparencies (measured at 550 nm) exhibited variable sheet resistance values depending on their composition and intrinsic electronic conductivity (see Table S1, ESI†). To further minimize the contact resistance between the MXene thin film and the graphite foil, mini binder clips (Office Depot brand) were used as shown in Video V1, ESI.†

Characterization

Dynamic light scattering (DLS) was performed by pipetting 1 mL of diluted colloid solution into a polystyrene cuvette (Zetasizer Nano ZS, Malvern Panalytical). DLS average was taken over a total of five measurements from each sample. Structural analysis of MXene films was performed by X-ray diffraction (XRD) using a Rigaku Smart Lab (Tokyo, Japan) diffractometer with Cu Kα radiation (voltage and current settings were 40 kV and 44 mA, respectively) with a step scan of 0.04°, 2θ range of 3–20° and a dwell time of 0.5 s. The lateral dimensions of MXene flakes and cross-sectional views of the MXene thin films were imaged using a scanning electron microscope (SEM, Zeiss Supra 50VP, Germany). The optical properties of MXene thin films were studied by UV-vis spectroscopy (Evolution 201 UV–vis–NIR spectrophotometer, Thermo-Fischer Scientific). The electrical conductivity and sheet resistance (at an applied current of 0.5 mA) of MXene thin films were measured by taking the average of sheet resistance values measured at five different locations of the film on four corners and center using a four-point probe conductivity meter (ResTest v1, Jandel Engineering Ltd, Bedfordshire, UK) with a probe distance of 1 mm.

Electrochemical testing. The electrochemical tests (cyclic voltammetry (CV) and chronoamperometry) were performed at room temperature using a VMP3 electrochemical workstation (BioLogic, France). Electrochromic MXene three-electrode cells were pre-cycled by performing CV in a stable potential window of −1 to 0 V (*vs.* Ag wire) for $Ti_3C_2T_x$, Ti_3CNT_x, Ti_2CT_x and −1 to −0.2 V (*vs.* Ag wire) for $Ti_{1.6}Nb_{0.4}CT_x$ at a scan rate of 20 mV s^{-1} for 5 cycles.

***In situ* UV-vis and electrochemical studies.** Cells made with glass substrates filled with an electrolyte (1 M H_3PO_4 or H_3PO_4/PVA gel) were used as a blank to correct for background before running UV-vis tests. To avoid leaks associated with liquid electrolytes during long-term UV-vis tests (*in situ* UV-vis combined with chronoamperometry and cyclic voltammetry), we employed protic gel electrolytes, while a liquid electrolyte was used for short-time tests (switching rate studies). The transmittance of MXene thin films and electrochromic cells

was recorded from 300 to 1000 nm with 1 nm step using deuterium and tungsten lamps. *In situ* UV–vis spectra were recorded by synchronous measurements of the UV–vis spectrophotometer with a Biologic SP 150 potentiostat. The electrochromic cell was placed in the spectrophotometer in such a way that the scratched area in the counter electrode aligned with the light path. In this case, the light only probes the MXene in the working electrode. The UV–vis spectra under different potentials (*vs.* Ag wire) were recorded at the end of each chronoamperometry cycle (holding at a fixed potential for 10 minutes) and during relaxation at open circuit voltage (OCV) after each potential step. These measurements were repeated with 100 mV increments until reaching −1 V (*vs.* Ag wire) from OCV during cathodic polarization and OCV to 0.1 V (*vs.* Ag wire) during anodic polarization. OCV is the condition of the electrochemical cell without application of voltage or current but having interfacial contact of the electrolyte with the MXene thin film. To monitor the change in transparency of the electrochromic system with cycling, while CV was performed in a stable window at a scan rate of 50 mV s^{-1}, transmittance at a particular wavelength (where there was a maximum transmittance change) was recorded. Similarly, switching rates were calculated by recording the transmittance change with alternative 0 and −1 V potential perturbations *vs.* Ag wire (chronoamperometry) for 20 s each. Switching time of MXene electrodes was calculated by estimating the time taken to attain 90% of the transmittance peak shift of ΔT.[15]

Conflicts of interest

There are no conflicts to declare.

Acknowledgements

G. V. was supported by the French Network RS2E through a scholarship for the master program Materials for Energy Storage and Conversion (M.E.S.C.). K. H. was supported by the U.S. Department of Energy (DOE), Office of Science, Office of Basic Energy Sciences, grant #DE-SC0018618. K. M. was supported by the Army Research Office under Cooperative Agreement Number W911NF-18-2-0026. Funding was provided by the U.S. Army *via* the Surface Science Initiative Program (PE 0601102A Project VR9) at the Edgewood Chemical Biological Center. Prof. Babak Anasori and Dr. Christopher E. Shuck are acknowledged for providing MAX phases. Dr. Ariana Levitt is acknowledged for proofreading the manuscript. The authors acknowledge the Core Research Facilities (CRF) at Drexel University for providing access to characterization tools.

References

1 P. Yang, P. Sun and W. Mai, *Mater. Today*, 2016, **19**, 394–402.
2 A. Azens and C. Granqvist, *J. Solid State Electrochem.*, 2003, **7**, 64–68.
3 R. J. Mortimer, *Annu. Rev. Mater. Res.*, 2011, **41**, 241–268.
4 K. Doblhofer, *Soft Mater.*, 2008, **6**, 156–156.
5 E. L. Runnerstrom, A. Llordés, S. D. Lounis and D. J. Milliron, *Chem. Commun.*, 2014, **50**, 10555–10572.
6 J. Peng, H.-H. Jeong, Q. Lin, S. Cormier, H.-L. Liang, M. F. L. De Volder, S. Vignolini and J. J. Baumberg, *Sci. Adv.*, 2019, **5**, eaaw2205.
7 A. Kristensen, J. K. W. Yang, S. I. Bozhevolnyi, S. Link, P. Nordlander, N. J. Halas and N. A. Mortensen, *Nat. Rev. Mater.*, 2017, **2**, 16088.
8 L. Shao, X. Zhuo and J. Wang, *Adv. Mater.*, 2018, **30**, 1704338.
9 M. Kanehara, H. Koike, T. Yoshinaga and T. Teranishi, *J. Am. Chem. Soc.*, 2009, **131**, 17736–17737.
10 D. T. Christiansen, S. Ohtani, Y. Chujo, A. L. Tomlinson and J. R. Reynolds, *Chem. Mater.*, 2019, **31**, 6841–6849.
11 H. Gu, C. Guo, S. Zhang, L. Bi, T. Li, T. Sun and S. Liu, *ACS Nano*, 2018, **12**, 559–567.
12 B. Anasori and Y. Gogotsi, *2D Metal Carbides and Nitrides (MXenes)*, Springer, Cham, 2019.
13 Y. Gogotsi and B. Anasori, *ACS Nano*, 2019, **13**, 8491–8494.
14 K. Hantanasirisakul and Y. Gogotsi, *Adv. Mater.*, 2018, **30**, 1804779.
15 P. Salles, D. Pinto, K. Hantanasirisakul, K. Maleski, C. E. Shuck and Y. Gogotsi, *Adv. Funct. Mater.*, 2019, **29**, 1809223.
16 F. Shahzad, M. Alhabeb, C. B. Hatter, B. Anasori, S. M. Hong, C. M. Koo and Y. Gogotsi, *Science*, 2016, **353**, 1137–1140.
17 Y. Dong, S. Chertopalov, K. Maleski, B. Anasori, L. Hu, S. Bhattacharya, A. M. Rao, Y. Gogotsi, V. N. Mochalin and R. Podila, *Adv. Mater.*, 2018, **30**, 1705714.
18 A. Sarycheva, A. Polemi, Y. Liu, K. Dandekar, B. Anasori and Y. Gogotsi, *Sci. Adv.*, 2018, **4**, eaau0920.
19 B. Anasori, M. R. Lukatskaya and Y. Gogotsi, *Nat. Rev. Mater.*, 2017, **2**, 16098.
20 M. Okubo, A. Sugahara, S. Kajiyama and A. Yamada, *Acc. Chem. Res.*, 2018, **51**, 591–599.
21 C. (John) Zhang and V. Nicolosi, *Energy Storage Mater.*, 2019, **16**, 102–125.
22 J. K. El-Demellawi, S. Lopatin, J. Yin, O. F. Mohammed and H. N. Alshareef, *ACS Nano*, 2018, **12**, 8485–8493.
23 G. Ying, S. Kota, A. D. Dillon, A. T. Fafarman and M. W. Barsoum, *FlatChem*, 2018, **8**, 25–30.
24 G. Ying, A. D. Dillon, A. T. Fafarman and M. W. Barsoum, *Mater. Res. Lett.*, 2017, **5**, 391–398.
25 K. Hantanasirisakul, M. Alhabeb, A. Lipatov, K. Maleski, B. Anasori, P. Salles, C. Ieosakulrat, P. Pakawatpanurut, A. Sinitskii, S. J. May and Y. Gogotsi, *Chem. Mater.*, 2019, **31**, 2941–2951.
26 M. Alhabeb, K. Maleski, B. Anasori, P. Lelyukh, L. Clark, S. Sin and Y. Gogotsi, *Chem. Mater.*, 2017, **29**, 7633–7644.
27 A. D. Dillon, M. J. Ghidiu, A. L. Krick, J. Griggs, S. J. May, Y. Gogotsi, M. W. Barsoum and A. T. Fafarman, *Adv. Funct. Mater.*, 2016, **26**, 4162–4168.
28 Y. Yang, K. Hantanasirisakul, N. C. Frey, B. Anasori, R. J. Green, P. C. Rogge, I. Waluyo, A. Hunt, P. Shafer,

E. Arenholz, V. B. Shenoy, Y. Gogotsi and S. J. May, *2D Mater.*, 2020, **7**, 025015.
29 X. Li, K. Perera, J. He, A. Gumyusenge and J. Mei, *J. Mater. Chem. C*, 2019, **7**, 12761–12789.
30 M. R. Lukatskaya, S.-M. Bak, X. Yu, X.-Q. Yang, M. W. Barsoum and Y. Gogotsi, *Adv. Energy Mater.*, 2015, **5**, 1500589.
31 R. Chapman and P. Mulvaney, *Chem. Phys. Lett.*, 2001, **349**, 358–362.
32 Y. R. Leroux, J. C. Lacroix, K. I. Chane-Ching, C. Fave, N. Félidj, G. Lévi, J. Aubard, J. R. Krenn and A. Hohenau, *J. Am. Chem. Soc.*, 2005, **127**, 16022–16023.
33 V. Stockhausen, P. Martin, J. Ghilane, Y. Leroux, H. Randriamahazaka, J. Grand, N. Felidj and J. C. Lacroix, *J. Am. Chem. Soc.*, 2010, **132**, 10224–10226.
34 Z. Wang and G. Chumanov, *Adv. Mater.*, 2003, **15**, 1285–1289.
35 D. Schaming, V.-Q. Nguyen, P. Martin and J.-C. Lacroix, *J. Phys. Chem. C*, 2014, **118**, 25158–25166.
36 J.-W. Jeon, P. A. Ledin, J. A. Geldmeier, J. F. Ponder, M. A. Mahmoud, M. El-Sayed, J. R. Reynolds and V. V. Tsukruk, *Chem. Mater.*, 2016, **28**, 2868–2881.
37 W. Lu, N. Jiang and J. Wang, *Adv. Mater.*, 2017, **29**, 1604862.
38 N. Jiang, X. Zhuo and J. Wang, *Chem. Rev.*, 2018, **118**, 3054–3099.
39 J. Tang, T. S. Mathis, N. Kurra, A. Sarycheva, X. Xiao, M. N. Hedhili, Q. Jiang, H. N. Alshareef, B. Xu, F. Pan and Y. Gogotsi, *Angew. Chem., Int. Ed.*, 2019, **58**, 17849–17855.
40 C. (John) Zhang, S. Pinilla, N. McEvoy, C. P. Cullen, B. Anasori, E. Long, S.-H. Park, A. Shmeliov, D. Krishnan, C. Morant, X. Liu, G. S. Duesberg, Y. Gogotsi and V. Nicolosi, *Chem. Mater.*, 2017, **29**, 4848–4856.
41 J. M. Luther, P. K. Jain, T. Ewers and A. P. Alivisatos, *Nat. Mater.*, 2011, **10**, 361–366.
42 Y. Zhao, H. Pan, Y. Lou, X. Qiu, J. Zhu and C. Burda, *J. Am. Chem. Soc.*, 2009, **131**, 4253–4261.
43 M. Han, C. E. Shuck, R. Rakhmanov, D. Parchment, B. Anasori, C. M. Koo, G. Friedman and Y. Gogotsi, *ACS Nano*, 2020, **14**, 5008–5016.
44 P. Salles, E. Quain, N. Kurra, A. Sarycheva and Y. Gogotsi, *Small*, 2018, **14**, 1802864.